A staggered double vane circuit for a W-band traveling-wave tube amplifier*

Lai Jian-Qiang(赖剑强)†, Wei Yan-Yu(魏彦玉), Liu Yang(刘 洋),
Huang Min-Zhi(黄民智), Tang Tao(唐 涛), Wang Wen-Xiang(王文祥), and Gong Yu-Bin(宫玉彬)

National Key Laboratory of Science and Technology on Vacuum Electronics, School of Physical Electronics, University of Electronic Science and Technology of China, Chengdu 610054, *China*

(Received 10 October 2011; revised manuscript received 28 November 2011)

Based on the combination of a staggered double vane slow wave structure (SWS) and round electron beam, a 200-W W-band traveling-wave tube (TWT) amplifier is studied in this paper. The main advantages of round beam operation over the sheet beam is that the round beam can be formed more easily and the focus requirement can be dramatically reduced. It operates in the fundamental mode at the first spatial harmonic. The geometric parameters are optimized and a transition structure for the slow wave circuit is designed which can well match the signal that enters into and goes out from the tube. Then a TWT model is established and the particle-in-cell (PIC) simulation results show that the tube can provide over 200-W output power in a frequency range of 88 GHz–103 GHz with a maximum power of 289 W at 95 GHz, on the assumption that the input power is 0.1 W and the beam power is 5.155 kW. The corresponding conversion efficiency and gain at 95 GHz are expected to be 5.6% and 34.6 dB, respectively. Such amplifiers can potentially be used in high power microwave-power-modules (MPM) and for other portable applications.

Keywords: traveling-wave tube, staggered double vane, slow wave structure, W-band

PACS: 84.40.Fe, 85.45.Bz, 84.30.Le **DOI:** 10.1088/1674-1056/21/6/068403

1. Introduction

Recently, scientists who dedicated their research to microwave sources and amplifiers have paid their attention to the millimeter and terahertz wave region.[1−5] Vacuum electronic devices (VEDs) are believed to be an important alternative to high-data-rate space communication, high power radar, and radiation sources for directed energy weapons, etc.[6] A traveling wave tube (TWT) amplifier is a kind of widely used VED that can provide high output power in a broad bandwidth.[7] Consequently, a great number of TWTs have been employed in many fields with frequency bands ranging from a few GHz to THz. The core part of the TWT is the slow wave structure (SWS) that can decelerate the phase velocity of the traveling wave in the RF circuit to a level approximately equal to the beam velocity.[8−10] Only then can the electromagnetic wave interact effectively with the electron beam so that it can be amplified.

A number of investigations have been conducted in the field of W-band TWT, however most of them can provide only the average output powers below 100 W.[11−15] Communications and Power Industries (CPI)[16] have made a periodic permanent magnet (PPM) focused 50-W CW TWT modeled VTW-6495A2 with an operation band of 93 GHz–95 GHz. Some devices can produce larger powers but with extremely limited bandwidths.[17,18]

The staggered double vane SWS has been investigated for many years and is believed to be a promising structure for high power millimeter and sub-millimeter wave amplifiers and oscillators. Shin and Barnett[19] studied the TWT operating at around 220 GHz based on a combination of the staggered double vane circuit and sheet beam. Their particle-in-cell (PIC) simulation results show that the TWT has a wide intrinsic bandwidth and a significant gain. However, the key challenge to realizing such a device is the formation and focus of the sheet beam, especially given that the high current density required for high power application makes a stumbling block to the beam transport. In this paper, we concentrate on the staggered double vane SWS for round beam W-band TWT with a mod-

*Project supported by the National Natural Science Foundation of China for Distinguished Young Scholars (Grant No. 61125103), the National Natural Science Foundation of China (Grant Nos. 60971038 and 60971031), and the Fundamental Research Funds for the Central Universities (Grant No. ZYGX2009Z003).

†Corresponding author. E-mail: LJQ6601@foxmail.com

© 2012 Chinese Physical Society and IOP Publishing Ltd

erate voltage (20.4 kV) and current (250 mA), which is comparatively technically easy to achieve. The fabrication scheme and magnetic stack for beam focus are planed for subsequent experimental study. The single period model of the SWS is analysed by the use of Ansoft HFSS.[20] The transmission characteristics of the tube and the PIC simulations are investigated with CST studio suite.[21]

2. Staggered double vane SWS

The staggered double vane SWS is predicted to have a strong symmetric axial electric field distribution along the electron beam propagation direction. It operates in the fundamental mode (TE_{10}) under the first spatial harmonic. The single period of the slow wave structure suitable for operating in the W-band is given in Fig. 1. To obtain the optimal structure size, various combinations of the dimensional parameters are involved in the calculations, which are done with the HFSS Eigenmode Solver based on master-slave boundary conditions.

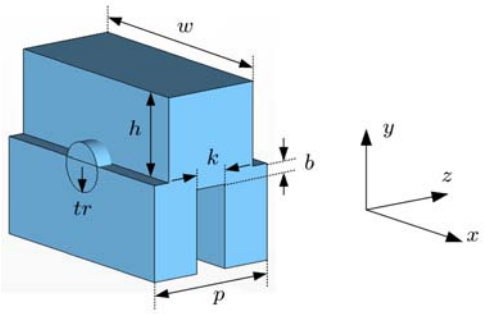


Fig. 1. (colour online) Three-dimensional schematic plot of a single period of the staggered double vane structure.

The design parameter $\varphi = k_z p = 2.5\pi$ is defined at a 95-GHz central frequency for phase synchronism with a beam accelerating voltage of about 21 kV. To provide a broad operation bandwidth and sufficient intrinsic volume for the beam–wave interaction with great interaction impedance, the geometrical circuit parameters designed for the +1 spatial harmonic operation are given in Fig. 1. The value of the period of p is derived as

$$\phi = k_z p = \frac{\omega}{V_p} p = (2\pi f_0 / V_p) p = 2.5\pi, \tag{1}$$

where ϕ is the defined phase shift, ω is the angular frequency, k_z is the phase constant and f_0 is the operation frequency (95 GHz). The variable V_p can be expressed as

$$V_p = \beta c = c\sqrt{1 - \frac{1}{(1 + V_0/5.11 \times 10^5)^2}}, \tag{2}$$

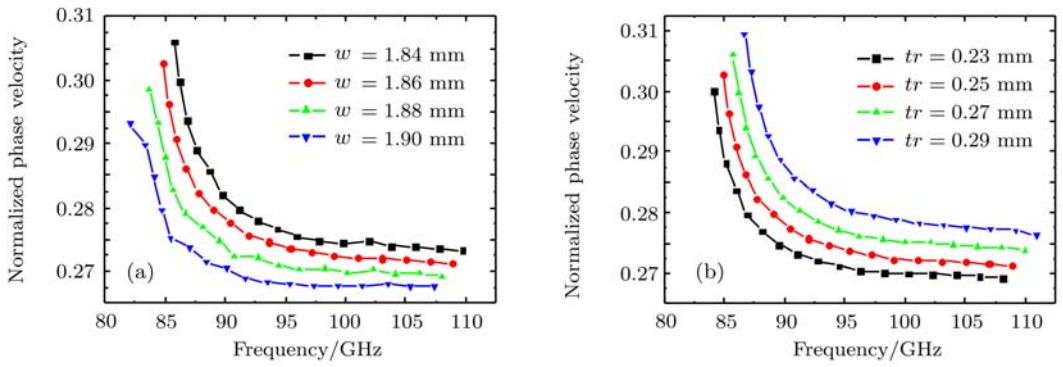
where c is the speed of light in a vacuum and V_0 is the synchronous voltage (about 21 kV). It is easy to attain that $p \approx 1.1$ mm. Other dimensional parameters are firstly assigned roughly and then determined with the help of numerical calculations.

Plotted in Fig. 2 are the dispersion curves with different dimensional parameter combinations. The optimal value of each parameter is picked out one by one through the corresponding simulations. Consequently, the optimized parameters for the structure are determined as $p = 1.1$ mm, $w = 1.86$ mm, $h = 0.68$ mm, $k = 0.27$ mm, $b = 0.12$ mm, and $tr = 0.25$ mm.

According to the definition given by

$$k_{cn} = \frac{|E_{zn}|^2}{2\beta_n^2 P_w}, \tag{3}$$

the interaction impedance of the SWS can be calculated, where P_w is the transmission power along the axial direction, E_{zn} and β_n are the amplitude of the axial-component of E-field and the phase constant on the n-th spatial harmonic, respectively. As many as 545 points on the cross section



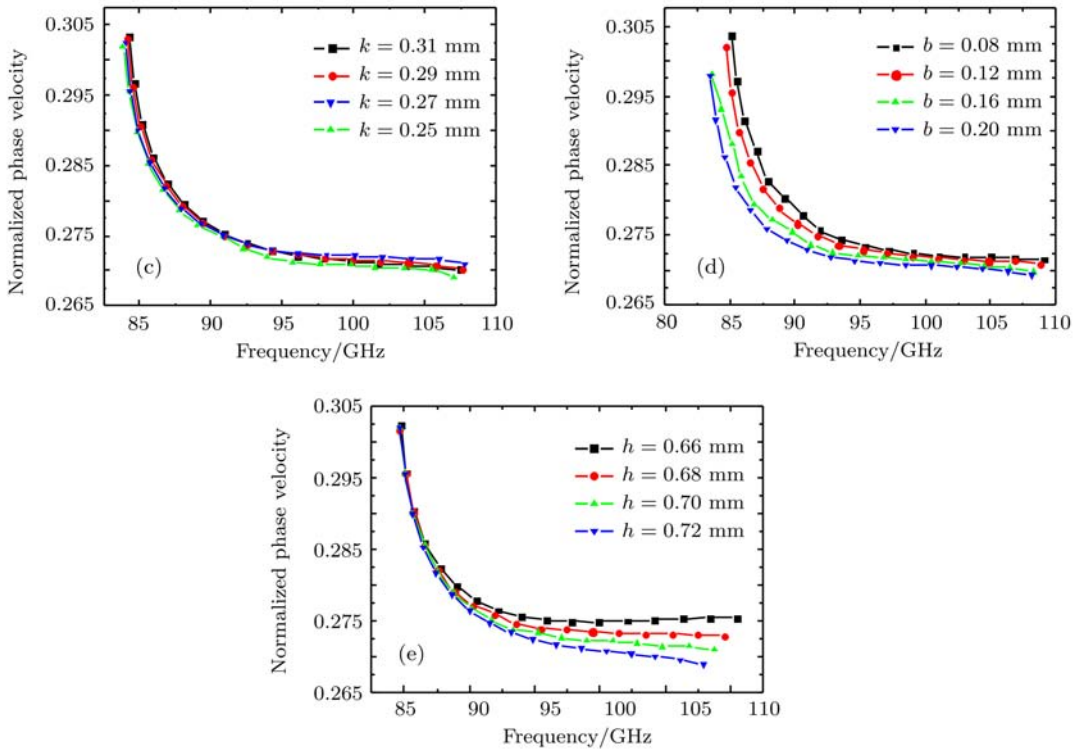


Fig. 2. (colour online) Dispersion curves of the staggered double vane SWS with combination of various dimensional parameters: (a) $b = 0.10$, $k = 0.29$, $h = 0.70$, $tr = 0.25$, $p = 1.1$; (b) $b = 0.10$, $k = 0.29$, $h = 0.70$, $w = 1.86$, $p = 1.1$; (c) $b = 0.10$, $h = 0.70$, $tr = 0.25$, $w = 1.86$, $p = 1.1$; (d) $k = 0.27$, $h = 0.70$, $tr = 0.25$, $w = 1.86$, $p = 1.1$; (e) $b = 0.12$, $k = 0.27$, $tr = 0.25$, $w = 1.86$, $p = 1.1$. The dimensional parameters are all in units of mm.

of the electron beam are involved in the calculation to evaluate the average interaction impedance as shown in Fig. 3. All the calculations in this paper are conducted with the assumption that the structure material is oxygen-free high-conductivity (OFHC) copper with the roughness of the structure surface taken into consideration, therefore the corresponding conductivity of the copper in W-band is $\sigma = 2.25 \times 10^7$ S/m.[17]

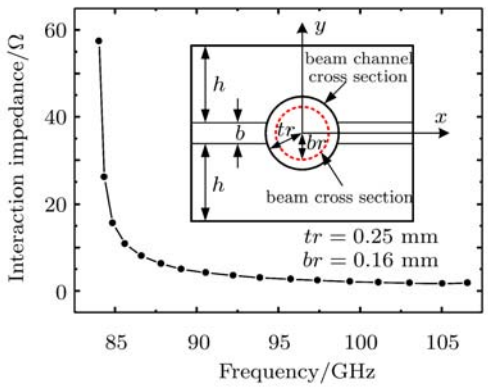


Fig. 3. (colour online) Average interaction impedance of the SWS. The values are obtained from 545 points uniformly distributed on the beam cross section.

3. Tube model and its performances

To match the RF signal entering into and going out from the SWS, a transition structure needs to be designed. Figure 4 gives the profile of a transition structure model,it can be seen that the vanes are closer to the input/output port, the heights (in the y direction) of the vanes decrease and the thickness of the vanes (in the z direction) increase. Consequently, there is a gradual transition from the RF circuit structure to a rectangular waveguide within a length of 5 SWS periods. The width (in the x direction) of the transition structure keeps unchanged with respect to the SWS.

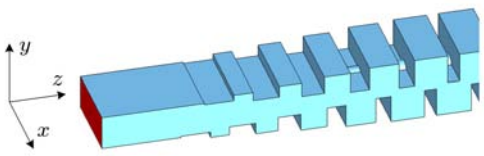


Fig. 4. (colour online) Transition structure for the SWS circuit of the tube.

Two transition structures together with 79 SWS periods constitute the TWT model as illustrated in Fig. 5(a). The wave guide ends of the two transition structures marked as port 1 and port 2 are the input port and the output port, respectively. The total length of the model is 102.3 mm, corresponding to the distance between port 1 and port 2. The transmission characteristics of the tube is calculated as plotted in Fig. 5(b), which demonstrates that the tube has a low reflection ratio ($S_{11} < -20$ dB) and a low transmission loss ($S_{21} > -2$ dB) in a broad frequency band range from 88 GHz to 103 GHz.

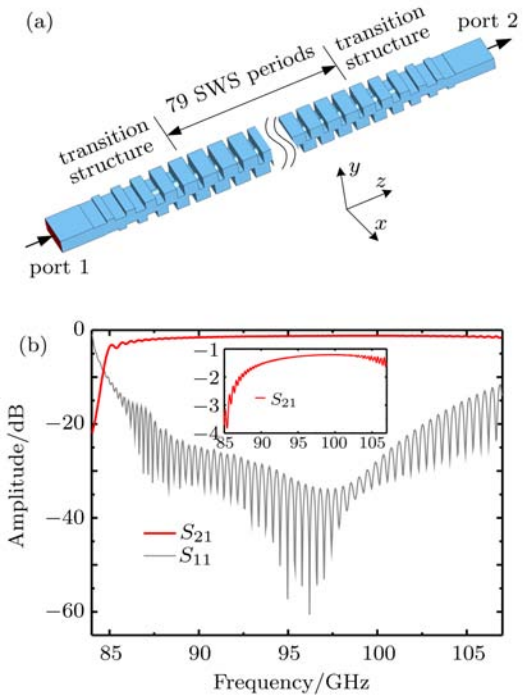


Fig. 5. (colour online) (a) Circuit model for the TWT, including 79 SWS periods and transition structures, and (b) the RF transmission characteristics of the tube model. The upper inset gives the detailed S_{21} curve.

After the determination of structure parameters of the RF circuit, the PIC simulation is conducted to investigate the amplification performance of the model. It is assumed that a pencil beam with a moderate current of 0.25 A and a cross section radius of 0.16 mm, as shown in the inset of Fig. 3, is injected into port 1. Simultaneously, a 95-GHz RF sinusoidal signal with a constant power of 0.1 W is input through port 1 for the PIC simulation. The operation voltage of the tube is 20.62 kV and the corresponding current density is 310.8 A/cm^2 with a beam filling ratio of 64%. A uniform axial magnetic field of 0.6 T is employed for the beam focus.

Figure 6 shows the PIC simulation results of the output and the reflected signal amplitude. As can be seen, the driven power is amplified to a steady value of 289 W, corresponding to a gain of 34.5 dB. The reflected power keeps lower than the input power after the 3.5-ns operation. Figure 7 shows the longitudinal power distribution in the circuit when the tube operates in a steady state. From Fig. 7, together with the phase space plot of the electrons as the inset, we can see the energy interaction process between the electron beam and electromagnetic wave. More information about the input, output, and reflected signals is described by the frequency spectra plotted in Fig. 8. As can be seen, the peak value of the reflected signal spectrum is approximately 9 dB smaller than that of the input signal spectrum. The output signal appears relatively pure around 95 GHz; despite the fact that the second and third harmonics, which are approximately 60 dB lower than the operation points at around 190 GHz and 285 GHz respectively, are observed. It should be pointed out that the powers described in this paper are all peak powers, so half the peak powers are their corresponding average powers.

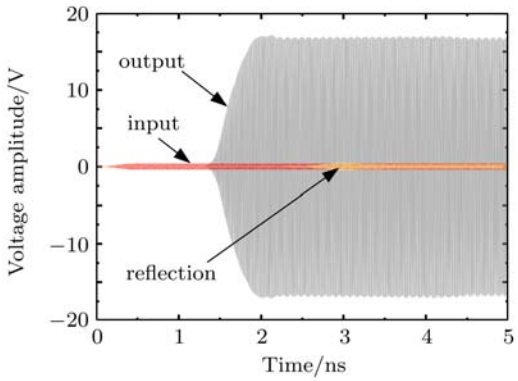


Fig. 6. (colour online) Voltage amplitudes of input, output, and reflected RF signals at 95 GHz.

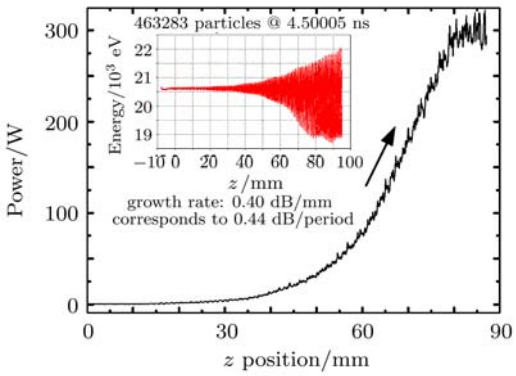


Fig. 7. (colour online) Power growth in the circuit along the axial direction. The inset shows the phase space plot of the electrons.

To verify the tube amplification performance in the transmission pass band predicted in Fig. 5(b), the driven signals with the frequency scan from 85 GHz to 107 GHz are included in the PIC simulations. The output power of the tube is given in Fig. 9. As can be seen, the frequency band over the 200-W output power ranges from 88 GHz to 103 GHz with a maximum power of 289 W and a gain of 34.6 dB at 95 GHz. The potential performance of the TWT is predicted from the design results, and deserves further investigation.

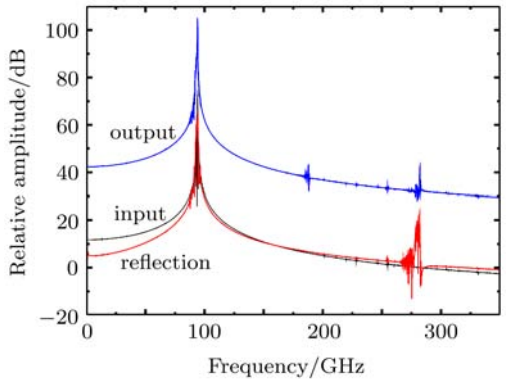


Fig. 8. (colour online) Frequency spectra of input, output, and reflected RF signals at 95 GHz.

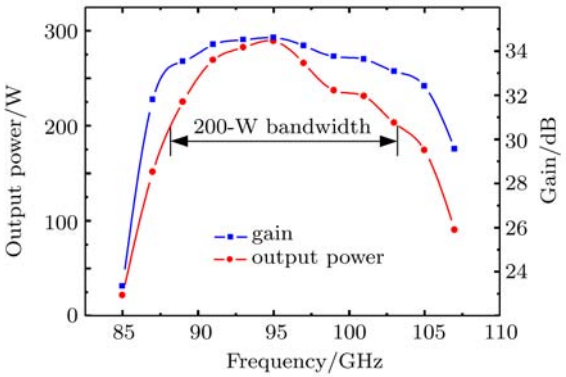


Fig. 9. (colour online) Output power and the corresponding gain versus frequency.

The gain-stability equation is used to judge the operation state.[22] Assume

$$J = G - L - \rho_{\mathrm{i}} - \rho_{\mathrm{o}}, \tag{4}$$

where G is the gain of the TWT, L is the loss of the circuit, and ρ_{i} and ρ_{o} are the reflection coefficients at the input and the output, respectively. If $J > 0$, the oscillation is believed to occur. On the assumption that the maximum gain is 34.6 dB, the lowest loss is -1.2 dB (S_{21}), and the reflection coefficient is S_{11}. The input and the output given in Fig. 6 are those in a worse case scenario, all the corresponding J values in a frequency range of 88 GHz–103 GHz are less than 0, indicating a stable operation. However, the tube model does not include the input/output couplers which may potentially lead to larger reflection coefficients, implying possible oscillation. A solution for this problem is to add attenuating material in the slow wave circuit. The scheme of an attenuator together with the coupler design can be consulted in our previous work.[23]

Future work is also in our schedule. Here, we will consider the use of the PPM configuration schematically as shown in Fig. 10(a), to achieve stable transport of the pencil beam with a voltage of 20.4 kV and a beam current of 250 mA. The RF circuit should be placed as a whole in the cylindrical tunnel enclosed by the periodic-permanent-magnetic (PPM) stack. The samarium cobalt (Sa–Co), which has remanence magnetic flux density $B_{\mathrm{r}} = 1.1$ T and relative permeability $\mu_{\mathrm{m}} = 1.05$,[24] is utilized for the magnet pole. Figure 10(b) shows the magnetic vector field distribution calculated by CST-PS Tracking. An electron gun including a tungsten dispenser cathode with a cathode loading of 16 A/cm^2 is also currently being studied.

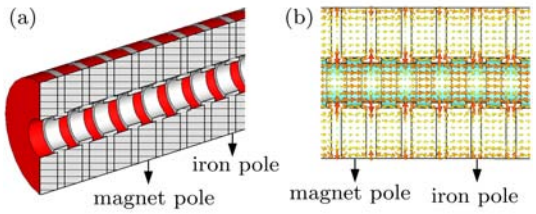


Fig. 10. (colour online) PPM configuration for beam focus: (a) three-dimensional diagram and (b) simulation result of the vector magnetic field distribution.

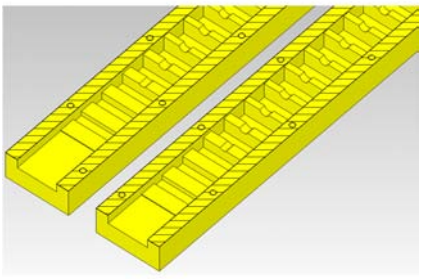


Fig. 11. (colour online) Fabrication plan for the circuit. Two similar structures would be machined and then combined by fastening bolts.

Fabrication of the pencil beam staggered double vane circuit will involve two steps. Two single vane circuit components should be machined separately and

each vane is grooved as seen in Fig. 11. The two parts should then be fixed together with fastening bolts or pins. The modern precision computerized numerical control (CNC) machine can easily fabricate the circuit structure, which enables future experiments.

4. Conclusion

A staggered double vane SWS combined with a round electron beam is applied to a W-band TWT amplifier providing over 200 W of output power. Compared with the sheet beam device based on similar circuit structures, the tube in this study dramatically reduces the requirements for beam formation and transportation. Calculation results demonstrate that the tube can operate in a frequency range of 88 GHz–103 GHz with an instantaneous bandwidth in excess of 15.7%. The maximum output power of this amplifier reaches 289 W at 95 GHz with a gain of 34.5 dB, corresponding to a growth rate of approximately 4 dB/cm. The magnetic stack and the circuit fabrication have been planed. Future work will include the designs of the coupler, RF windows, and attenuator.

References

[1] Qiu J X, Levush B, Pasour J, Katz A, Armstrong C M, Whaley D R, Tucek J, Kreischer K and Gallagher D 2009 *IEEE Microw. Mag.* **10** 38

[2] Li Z Y, Yao J Q, Xu D G, Zhong K, Wang J L and Bing P B 2011 *Chin. Phys.* B **20** 054207

[3] Booske J H, Dobbs R J, Joye C D, Kory C L, Neil G R, Park G S, Park J and Temkin R J 2009 *IEEE Trans. Terahertz Sci. Tech.* **56** 713

[4] He J, Wei Y Y, Gong Y B, Duan Z Y and Wang W X 2010 *Acta Phys. Sin.* **59** 2843 (in Chinese)

[5] Liu W X, Huang W H, Du Y C, Yan L X, Wu D and Tang C X 2011 *Chin. Phys.* B **20** 074102

[6] Cascone M 2008 *Proc. IEEE Int. Vac. Electron. Conf.*, April 22–24, 2008 Monterey, USA p. 12

[7] Hu Y L, Yang Z H, Li J Q, Li B, Gao P and Jin X L 2009 *Acta Phys. Sin.* **58** 6665 (in Chinese)

[8] Zhang C Q, Gong Y B, Wei Y Y and Wang W X 2010 *Acta Phys. Sin.* **59** 6653 (in Chinese)

[9] Peng W F, Hu Y L, Yang Z H, Li J Q, Lu Q R and Li B 2011 *Chin. Phys.* B **20** 028401

[10] Du C H, Liu P K and Xue Q Z 2010 *Acta Phys. Sin.* **59** 4611 (in Chinese)

[11] Feng J J, Hu Y F, Cai J, Ma S Y and Wu X P 2010 *Proc. IEEE Int. Vac. Electron. Conf.*, May 21–24, 2010, Monterey, USA p. 501

[12] Feng J J, Hu Y F, Cai J, Wu X P and Tang Y 2010 *Vacuum Electronics* **2** 27 (in Chinese)

[13] Kory C, Ives R L, Read M, Booske J, Jiang H, van der Walls D, Ho S J, Sengele S and Phillips P 2006 *Proc. IEEE Int. Vac. Electron. Conf.*, April 25–27, 2006, Monterey USA p. 447

[14] Gerum W, Lippert G, Malzahn P and Schneider K 2001 *IEEE Trans. Electron Dev.* **48** 72

[15] Kory C L, Dayton J A, Mearini G T Jr, Malta D, Lueck M, Gilchrist K and Vancil B 2009 *Proc. IEEE Int. Vac. Electron. Conf.*, April 28–30, 2009, Rome, Italy p. 125

[16] Communication and Power Industry, Model VTW-6495A2, online available: www.cpii.com

[17] Kory C L, Read M E, Ives R L, Booske J H and Borchard P 2009 *IEEE Trans. Electron Dev.* **56** 713

[18] Theiss A J, Meadows C J, Freeman R, True R B, Martin J M and Montgomery K L 2010 *IEEE Trans. Plasma Sci.* **38** 1239

[19] Shin Y M and Barnett L R 2008 *Appl. Phys. Lett.* **92** 091501

[20] Ansoft Corp., *Ansoft HFSS User's Reference*, online available: http://www.ansoft.com.cn/

[21] CST Corp., *CST MWS Tutorials*, online available: http://www.cst-china.cn/cst2009/

[22] Gilmour A S Jr 1994 *Principles of Traveling-Wave Tubes* (Boston, Norwood, MA: Artech House) p. 218

[23] Lai J Q, Gong Y B, Xu X, Wei Y Y, Duan Z Y, Wang W X and Feng J J 2012 *IEEE Trans. Electron Dev.* **59** 496

[24] Wang J X, Barnett L R, Luhmann N C Jr, Shin Y M and Humphries S 2010 *Phys. Plasmas* **17** 043111